Comparative Study of Stearic Acid/Iron-Oxide Binary and Stearic Acid/Iron-Oxide/Titanium-Oxide Ternary for Use as Energy Storage Material

Rizky Andiarto[1)], Muhammad Khalish Nuryadin[1)], Rosari Saleh[1, a)]
[1]Departemen Fisika, Fakultas MIPA-Universitas Indonesia, 16424 Depok, Indonesia
[2]Integrated Laboratory of Energy and Environment, Fakultas MIPA-Universitas Indonesia,1624 Depok, Indonesia

[a]Corresponding's author: rosari.saleh@gmail.com, rosari.saleh@ui.ac.id

Abstract. In this work, a series of stearic acid/Fe_3O_4, and stearic acid/Fe_3O_4/TiO_2 nanocomposites for thermal energy storage (TES) system were synthesized through a two-step process. Fe_3O_4 nanoparticles and Fe_3O_4/TiO_2 nanocomposites were first prepared using sol-gel methods and then both samples were mixed into stearic acid by dispersion technique at three different weight % ratio to stearic acid: 5%, 10% and 15% to obtain stearic acid/Fe_3O_4, and stearic acid/Fe_3O_4/TiO_2 nanocomposites. Morphologies and structural properties of the samples were characterized by X-ray diffractometer (XRD), Fourier transform infrared spectroscopy (FTIR), field emission scanning electron microscope (FESEM) and energy dispersive X-ray spectroscopy (EDX), while thermal properties of the sample were determined by differential scanning calorimetry (DSC) and thermogravimetric analysis (TGA). The XRD patterns demonstrate, that stearic acid/Fe_3O_4 contained characteristic peaks of Fe_3O_4 and stearic acid structures, while peaks corresponded to anatase TiO_2 structures appear in stearic acid/Fe_3O_4/TiO_2 nanocomposites. From the DSC measurements, it is found that the maximum latent heat was found at samples with weight ratio of 5%. Moreover, the enhancement up to 20% of latent heat in solidifying as well as melting processes was observed. TGA measurements show high degradation temperature in the range of 246 - 251°C. The TGA results also shows that the residual mass of the sample matches the composition of Fe_3O_4 and Fe_3O_4/TiO_2 which is added to the stearic acid.

1. Introduction

Phase change materials (PCMs) employing in latent thermal energy storage (LTES) system is the most popular technique due to its ability to reduce the imbalance between the demand and the supply of energy [1-3]. As organic PCM, stearic acid (Sa) has been recommended as one of the most reliable thermal energy storage material due to its distinctive features like high storage density for given volume, nontoxic, and noncorrosive behavior [4-5]. However, for heat storage application, Sa as organic phase change material have low thermal conductivity and therefore limits their utility for large-scale application [6]. To overcome the problem, various strategies and approaches have been introduced to improve the ability of PCM to store and release heat, such as introducing metal fins, metal screen, and other metal structures. Unfortunately, these efforts resulted in limited enhancement [7-9].

Recently, some researchers have focused on dispersing nanomaterials into the PCM to enhance its ability to store and release heat [10-14]. Sahan et al. [15], studied the effect of the Fe_3O_4 nanoparticles

addition in paraffin and found that the latent heat of the paraffin as a phase change material increased. Another study by Jifen et al. [16], stated that, the addition of TiO_2 nanoparticle in paraffin may enhance the latent heat ability. Both Fe_3O_4 and TiO_2 nanoparticle addition by these study proved that nanoparticle could enhanced PCM ability to store and release heat. Therefore, In this research, metal oxide Fe_3O_4 nanoparticles and Fe_3O_4/TiO_2 nanocomposites were synthesized by sol gel method for used as an additive materials for stearic acid (Sa) as phase change material to form Sa/Fe_3O_4 binary and Sa Fe_3O_4/TiO_2 ternary mixture. TiO_2 nanoparticles in Fe_3O_4/TiO_2 nanocomposites were prepared with molar ratio of Fe_3O_4 : TiO_2 was 1:5. The structural, morphology and thermal properties of stearic acid Fe_3O_4 and stearic acid Fe_3O_4/TiO_2 nanocomposites were investigated.

2. Experimental Setup

In this research, Iron (II) sulfate heptahydrate ($FeSO_4.7H_2O$,99), sodium hydroxide (NaOH), ethanol, ethylene glycol (EG), titanium dioxide and stearic acid ($C_{17}H_{35}CO_2H$) as a phase change material were purchased form Merck and were used without purification. All of the chemical reagents were of analytical grade. Fe_3O_4 nanoparticles and Fe_3O_4/TiO_2 nanocomposites were synthesized using same method as explained by our previous study [17]. Binary and ternary mixtures of Sa/Fe_3O_4 and $Sa/Fe_3O_4/TiO_2$ were synthesized by dispersing desired amount of nanoparticle and nanocomposite in stearic acid (5, 10, 15 wt%). All of the dispersion technique were done by using sonification water bath at 69°C for 2h. The flow chart of sample synthesize process were shown in Figure 1.

The structural properties, morphologies and elemental analyses of the samples were characterized by X-ray Diffraction (XRD), Field Emission Scanning Electron Microscope (FESEM), Energy-Dispersive X-ray spectroscopy (EDX) and Fourier Transform Infrared Spectroscopy (FTIR). The thermal properties of the sample were measured by Differential Scanning Calorimetry (DSC) to observe melting and solidification behavior and Thermal Gravimetric Analyzer (TGA) to observe sample degradation temperature.

3. Results and Discussion

XRD is an effective tool to characterize the crystal structure. The XRD patterns of Sa/Fe_3O_4 and $Sa/Fe_3O_4/TiO_2$ nanocomposites with various amounts of Fe_3O_4 nanoparticle and Fe_3O_4/TiO_2 nanocomposite in Sa (5, 10, 15 wt%) are presented in Figure 2. This figure also shown the XRD patterns of pure Fe_3O_4 and TiO_2 nanoparticles as well as pure Sa. The XRD peaks at $2\theta = 30.2^o$, 35.5^o, 53.4^o, and 57.0^o of pure Fe_3O_4 nanoparticles are attributed to the crystalline planes of inverse

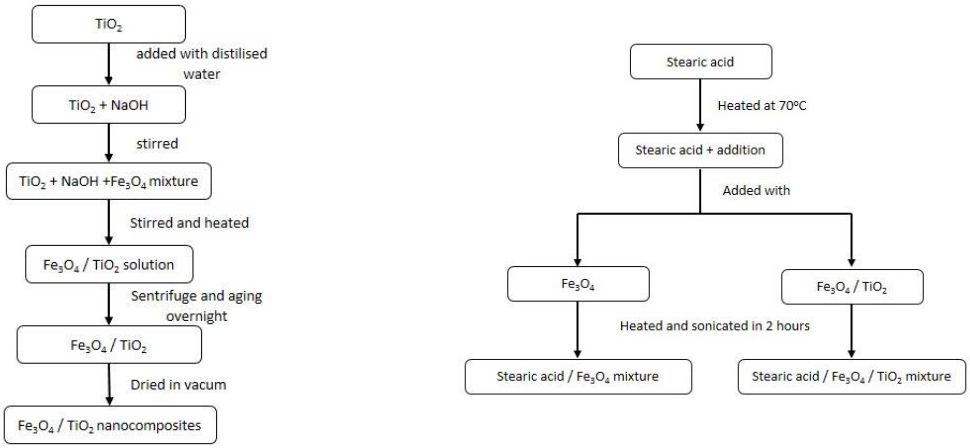

(a) (b)

Figure.1. Synthesize process flowchart of (a) Fe_3O_4 / TiO_2 nanocomposite, (b) stearic acid / Fe_3O_4 and stearic acid / Fe_3O_4 / TiO_2 mixture

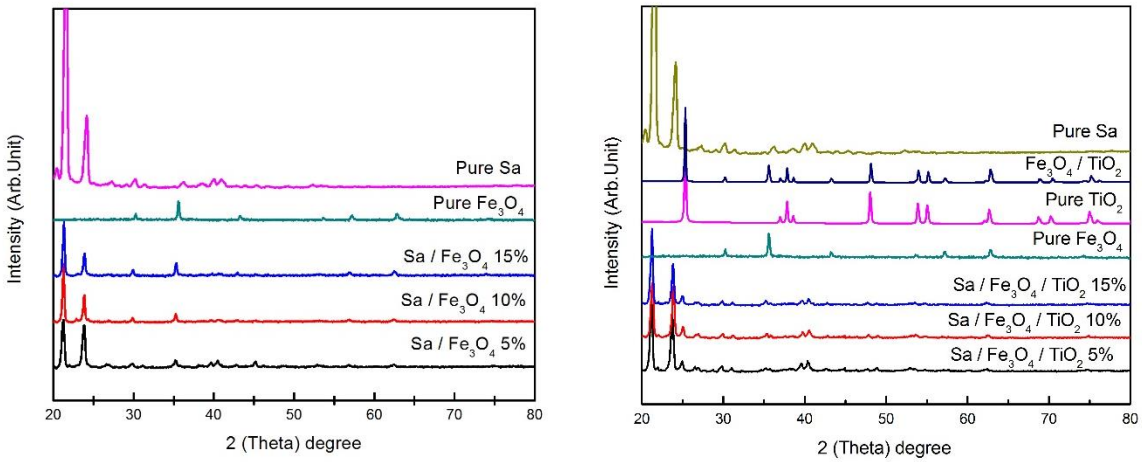

Figure. 2. (a) XRD patterns of Sa/Fe_3O_4 binary mixtures with various wt%, (b) XRD patterns of Sa/Fe3O_4/TiO_2 ternary mixtures with various wt%

cubic spinel structure at (220), (311), (511) and (440), while the XRD pattern of pure TiO_2 shows peaks at 2θ = 25.4°, 37.9 °, 48.1°, 54.2°, 55.1°, 62.6° and 75.1° corresponded to the crystalline planes of tetragonal anatase structure at (101), (004), (200), (105), (211), (204), and (215). The XRD peaks at 21.3° and 24.7° of the Sa are due to its regular crystallization. The XRD pattern of Fe_3O_4 /TiO_2 nanocomposites show the reflection peaks can be readily indexed to a combination of reflection peaks that can be ascribed to cubic spinel Fe_3O_4 and anatase TiO_2. The absence of other mixtures of Fe_3O_4 and TiO_2 diffraction peaks in the spectra confirms that the nanocomposites were the desired materials, Fe_3O_4/TiO_2.

As can be seen in Figure 2b, all peaks shown in Fe_3O_4, Fe_3O_4/TiO_2 and the prominent peaks of Sa are also shown in the XRD spectra of Sa/Fe_3O_4 and Sa/Fe_3O_4/TiO_2 nanocomposites. The peaks of Fe_3O_4 nanoparticles in Sa/Fe_3O_4 were slightly increased as the amounts of Fe_3O_4 nanoparticles dispersed in Sa were also increased. The same results were also found in Sa/Fe_3O_4/TiO_2 nanocomposites. The peak at 25° which corresponds to the presence of TiO_2 nanoparticles increased as the concentrations of nanocomposites in Sa were also increased.

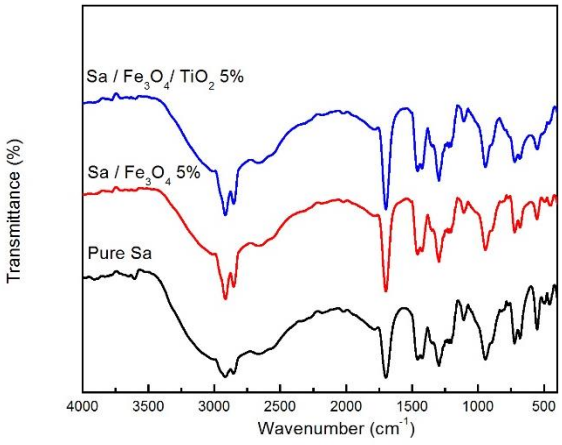

Figure. 3. FTIR spectra of Sa/Fe_3O_4 and Sa/Fe_3O_4/TiO_2

Figure 3 shows FTIR measurement of pure Sa, Sa/Fe_3O_4, and Sa/Fe_3O_4/TiO_2 mixtures. The transmittance at 2917 cm^{-1}, 2849 cm^{-1}, and 1703 cm^{-1} show the stretching vibration of CH_3, CH_2, and C=O molecules respectively. While 1464 cm^{-1}, 1296 cm^{-1}, 934 cm^{-1} and 720 cm^{-1} correspond to in plane, out of plane and in plane swinging of OH molecules respectively. There are neither Fe_3O_4 or TiO_2

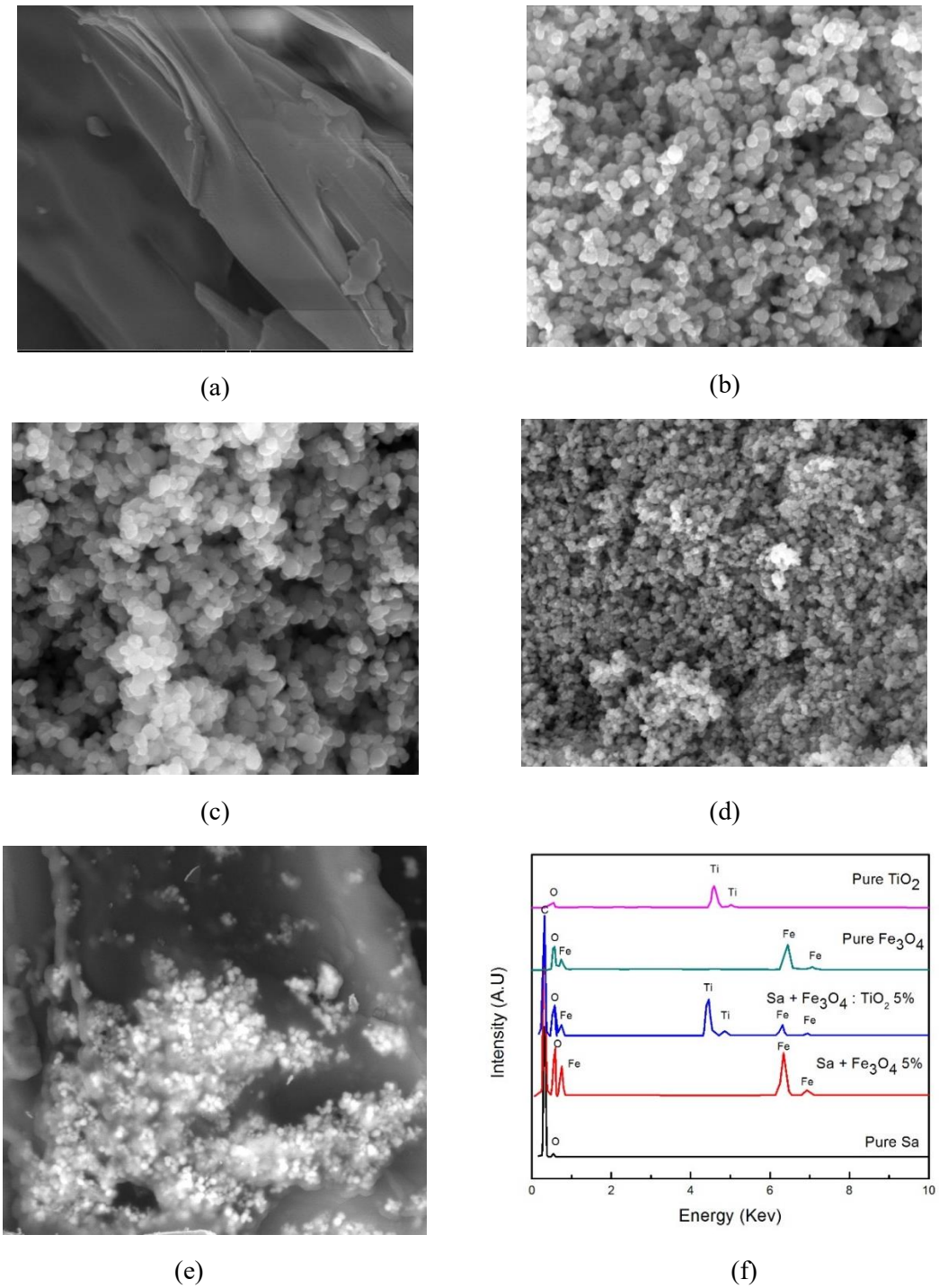

Figure. 4. FESEM images of (a) pure Sa, (b) pure Fe_3O_4 nanoparticle, (c) pure TiO_2 nanoparticle, (d) Fe_3O_4/TiO_2 nanocomposites, (e) Sa/Fe_3O_4/TiO_2 ternary mixture, (f) Corresponding EDX spectra of Sa / Fe_3O_4 and SaFe_3O_4/TiO_2

transmittance that can be found in the FTIR spectrum because the small amount of Fe_3O_4 and TiO_2 which are dispersed in Sa. However, the same value of transmittance wavenumber spectrum indicates that there are no chemical interaction between the Sa and nanoparticles/nanocomposite materials which can disrupts the phase change material itself [18].

Figure 4 shows the FESEM images of Fe_3O_4 and TiO_2 nanoparticles, Fe_3O_4/TiO_2 nanocomposites, pure Sa, and $Sa/Fe_3O_4/TiO_2$ nanocomposites. FESEM images revealed that pure Fe_3O_4 and TiO_2 as well as Fe_3O_4/TiO_2 nanocomposites have spherical-like shapes [17], while $Sa/Fe_3O_4/TiO_2$ nanocomposites showed the distribution of nanoparticles on the top of Sa.

In order to detect the atomic composition of the Sa/Fe_3O_4 and $Sa/ Fe_3O_4/TiO_2$ nanocomposites, the EDX spectroscopy was performed and the resulting spectra were displayed in Figure 3f. The EDX analysis confirmed that the Sa/Fe_3O_4 nanocomposites measurement consist of C, Fe, and O atoms while the $Sa/Fe_3O_4/TiO_2$ nanocomposites measurement consist of C, Fe, Ti, and O atoms. This result supports the presence Fe_3O_4 and TiO_2 by XRD measurement.

Thermal characteristics of all samples were studied with the DSC in terms of phase change temperature and latent heat. In the DSC measurements, the melting and solidifying onset temperature and peak temperature as shown in Figure 5 were observed. The onset point of melting and solidification process were determined by intersection between the slope and baseline of the curve while the peak temperature of melting and solidification point were determined by the highest and lowest peak of the DSC curve. Latent heat value of DSC measurement was calculated by integrating area under the peak of melting and solidifying process. The phase-change-characteristic data derived from DSC experiments are summarized in Table.1. As can be seen in Table.1, with the addition of Fe_3O_4 nanoparticles and Fe_3O_4/TiO_2 nanocomposites, there is no significant change in the onset temperature which the sample start to melt as well as peak temperature which shows complete process of melting. Similar things were also found in solidifying process. These results indicated that the phase change temperature process is not disrupted by addition of nanoparticle and nanocomposite.

It is known that latent-heat as a thermal property of phase change material is the most important parameters for a latent heat thermal storage system. This parameter shows the ability on how much phase change material absorbs and releases heat [19]. Based on the latent heat calculation of DSC curve in Figure 5, the presence of Fe_3O_4 nanoparticles and Fe_3O_4/TiO_2 nanocomposites were found to enhance the value of latent heat. As can be seen in Figure.6, The enhancement was found to be maximum at the addition of 5wt% of Fe_3O_4 nanoparticles and Fe_3O_4/TiO_2 nanocomposites in Sa. Moreover, the enhancement up to 20% of latent heat in solidifying as well as melting processes was observed in the

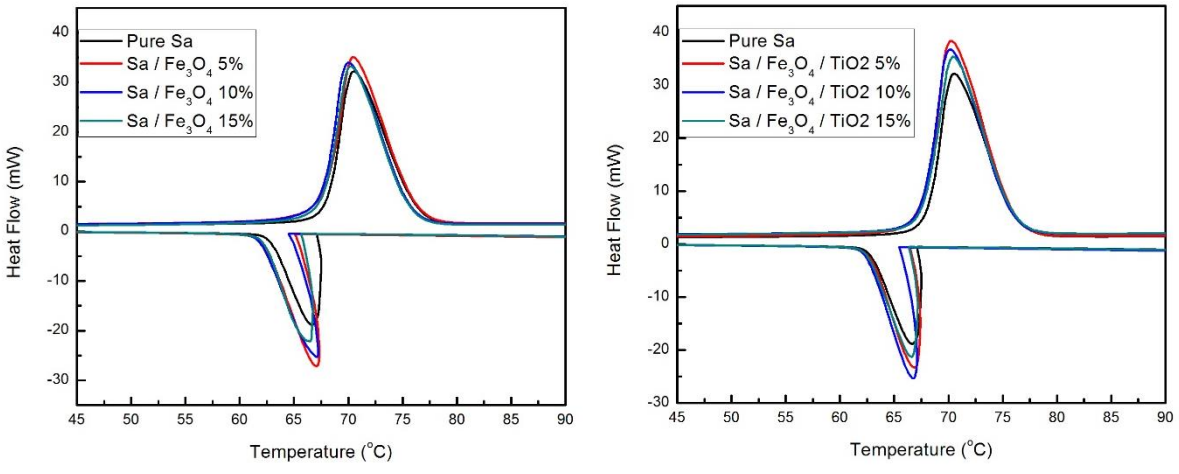

Figure. 5. Corresponding DSC curves with all various wt% of (a) Sa/Fe_3O_4, (b) $Sa/Fe_3O_4/TiO_2$

Table 1. solid-liquid, liquid-solid phase change temperature, melting, and solidifying latent heat data based on DSC measurement in Sa/Fe_3O_4 and Sa/Fe_3O_4/TiO_2

Sample Name	Solid- Liquid (°C)		Liquid-Solid (°C)		Melting Latent Heat	Solidifying Latent Heat
	Onset	peak	Onset	peak	(J/g)	(J/g)
Sa	67.7	70.5	67.2	66.6	177.635	174.135
Sa/$Fe_3O_4$5%	67.4	70.4	64.6	66.6	196.803	193.303
Sa/$Fe_3O_4$10%	67.2	70.2	63.5	66.1	188.169	184.669
Sa/$Fe_3O_4$15%	67.3	70.1	65.1	66	178.344	174.844
Sa/Fe_3O_4/5$TiO_2$5%	67.3	70.3	65.5	66.9	214.269	209.407
Sa/Fe_3O_4/5$TiO_2$10%	67.2	70.2	66.5	66.8	200.41	196.24
Sa/Fe_3O_4/5$TiO_2$15%	67.4	70.4	66.4	66.6	196.884	192.992

addition of Fe_3O_4/TiO_2 nanocomposites. The possible reason for the increment in latent heat is due to the molecular attraction between nanoparticles and Sa [20]. With this enhanced latent heat value, Sa/Fe_3O_4 and Sa/Fe_3O_4/TiO_2 nanocomposites developed a good candidate for latent heat thermal storage system.

Thermal stability of the sample was also measured by thermogravimetric analysis. As can be seen in Figure 7, all of the samples exhibit strong thermal stability up to 200°C. In table.2, the pure Sa degradation starts at 251°C with 100% weight loss. The addition of Fe_3O_4 nanoparticles and Fe_3O_4/TiO_2 nanocomposites in Sa didn't cause any favorable effect on the degradation process. However, the value of percentage loss in the Table.2 provides an information about the residual mass of the sample. Based on the results, it can be concluded that the residual mass of all the samples match the composition of Fe_3O_4 nanoparticles and Fe_3O_4/TiO_2 nanocomposites which is added into the Sa.

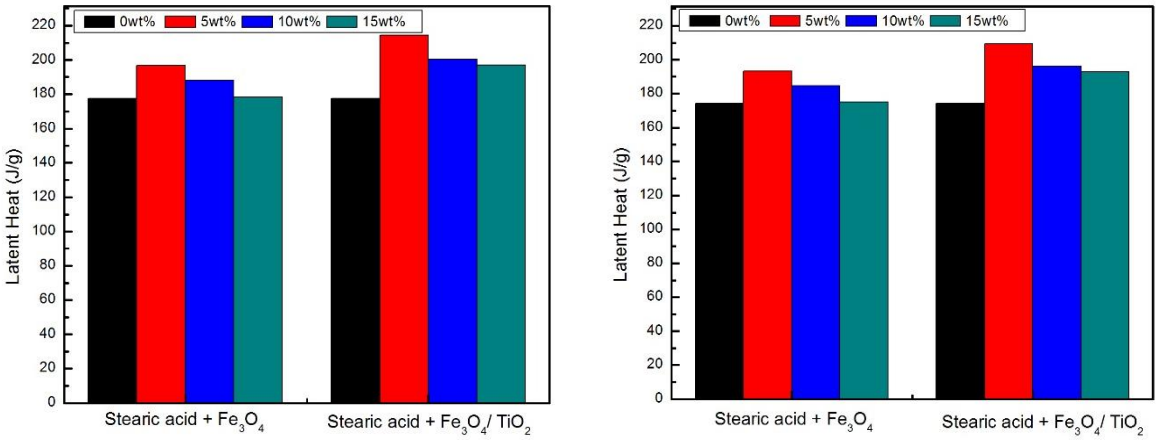

Figure. 6. Latent heat of Sa/Fe_3O_4 and Sa/Fe_3O_4/TiO_2 with all various wt% in (a) melting process, (b) solidifying process

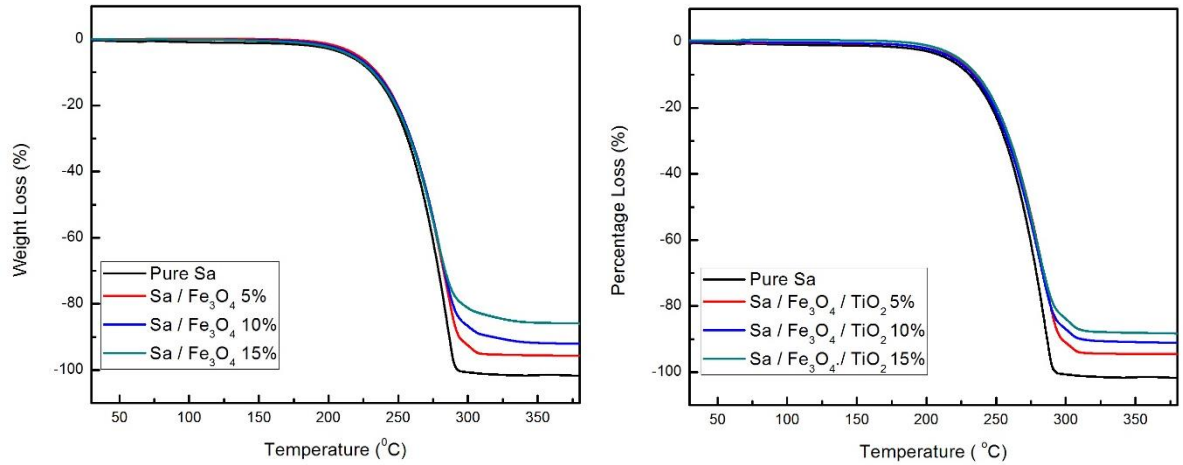

Figure. 7. Corresponding TGA curves with all various wt% of (a) Sa/Fe_3O_4, (b)Sa/Fe_3O_4/TiO_2

Table 2. Onset temperature and percentage loss of Sa/Fe_3O_4 and Sa/Fe_3O_4/TiO_2 samples

Sample Name	Onset Temperature (°C)	Percentage Loss (%)
Sa	251.6	100%
Sa/$Fe_3O_4$5%	251.5	94.49%
Sa/$Fe_3O_4$10%	250.8	90.26%
Sa/ $Fe_3O_4$15%	250.1	86.75%
Sa/ Fe_3O_4/5$TiO_2$5%	250.3	93.37%
Sa/ Fe_3O_4/5TiO210%	249.7	90.86%
Sa/ Fe_3O_4/5$TiO_2$15%	249.6	85.15%

4. Conclusion

Fe_3O_4 nanoparticles and Fe_3O_4/TiO_2 nanocomposites were synthesized using sol gel method and were dispersed into stearic acid (Sa) using dispersion technique. Based on the XRD data, the structure of Fe_3O_4 nanoparticle was inverse cubic spine while the structure of TiO_2 was anatase. Both XRD and EDX measurement confirmed the presence of Fe_3O_4 and Fe_3O_4/TiO_2. FESEM results show that Fe_3O_4 and Fe_3O_4/TiO_2 was attached on top of stearic acid (Sa). Based on the DSC results, it is found that the maximum latent heat was found at 5 wt.% of nanoparticles and nanocomposites in Sa. Moreover, the enhancement up to 20% of latent heat in solidifying as well as melting processes was observed in the addition of Fe_3O_4/TiO_2 nanocomposites with melting and solidification point in the range of 65-69°C. by these results, the ability of Sa to absorb and release heat were found to be enhanced by the presence of the Fe_3O_4 and Fe_3O_4 / TiO_2 nanocomposites. TGA measurement shows right composition of Fe_3O_4 and Fe_3O_4 in Sa with high thermal decomposition temperature.

References

[1] A. Sharma, V.V Tyagi, C.R. Chen, et al., Renewable and Sustainable Energy Reviews 13 (2009) 318-345
[2] M.M. Farid, A.M. Khudhair, S.A.K. Razack, et.al., Energy Conervation and management 45 (2004) 1597-1615
[3] B.Zalba, J.M marin, L.F. Cabeza, et al., Applied Thermal Engineering 23 (2003) 251-283
[4] B.Li, T.Liu, L.Hu, Y.Wang, S.Nie. Chemical Engineering 215 (2013) 819-826
[5] L.Cao, Y.Tang, G.Fang. Energy 80 (2014) 98-103
[6] Z.Chen, L.Cao, G.Fang. Energy and Buildings 62 (2013) 469-474
[7] A.Castell, C.Sole, M.Medrano, et-al., Applied Thermal Engineering 28 (2008) 1676-1686
[8] C.Y. Zhao, W.Lu, Y.Tian, Solar Energy 84 (2010) 1402-1412
[9] A.Castel, C.Sole, M.Medrano, et-al., Journal of Building Performance Simulation 3 (2010) 245-254
[10] L.Chai, X. Wang, D. Wu, Applied Energy 138 (2015) 661-674
[11] H. Zhang, X. Wang, D. Wu, Journal of Colloid and Inerface Science 343 (2010) 246-255
[12] N. Sahan, M. Fois, H. Paskoy, Solar Energy Materials & Solar Cells 137 (2015) 61-67
[13] L.Cao, F. Tang, G.Fang, Energy & Buildings 72 (2014) 31-37
[14] F.Jiang, X. Wang, D. Wu, Applied Energy 134 (2014) 456-468
[15] N. Sahan, H.O Paskoy, Solar Energy Materials & Solar Cells 126 (2014) 56-61
[16] J.Wang, H.Xie, Z.Guo, L.Guan, Y.Li, Applied Thermal Engineering 73 (2014) 1541-1547
[17] S.A. Arifin, S. Jalaludin, R. Saleh, Advanced Materials research 1123 (2015) 264-269
[18] S. Harikrishnan, S.Magesh, S.Kalaiselvam, Thermochimica Acta 565 (2013) 137-145
[19] A.F. Regin, S.C. Solanki, J.S. Saini, Renewable and Sustainable Energy Reviews 12 (2008) 2438-2458
[20] S.Shaikh, K.Lafdi, K.Hallinan, Journal of Applied Physics 103 094302 (2008)